Journal of Materials Chemistry C

Plasmonic-enhanced polymer photovoltaic cells based on Au nanoparticles with wide absorption spectra of 300-1000 nm

Journal:	*Journal of Materials Chemistry C*
Manuscript ID:	TC-ART-05-2014-001004.R2
Article Type:	Paper
Date Submitted by the Author:	05-Sep-2014

Complete List of Authors:	Zhang, Yupei; Nanjing University of Posts and Telecommunications, Institute of Advanced Materials Chen, Shu-Fen; Nanjing University of Posts and Telecommunications, Institute of Advanced Materials Hao, Yu Li, Xue; Nanjing Institute of Technology, Mechanical Engineering Institute Huang, Wei; Nanjing University of Posts and Telecommunications, Institute of Advanced Materials Li, Xingao; Nanjing University of Posts and Telecommunications, Institute of Advanced Materials Wang, Lian-Hui; Nanjing University of Posts and Telecommunications, Institute of Advanced Materials

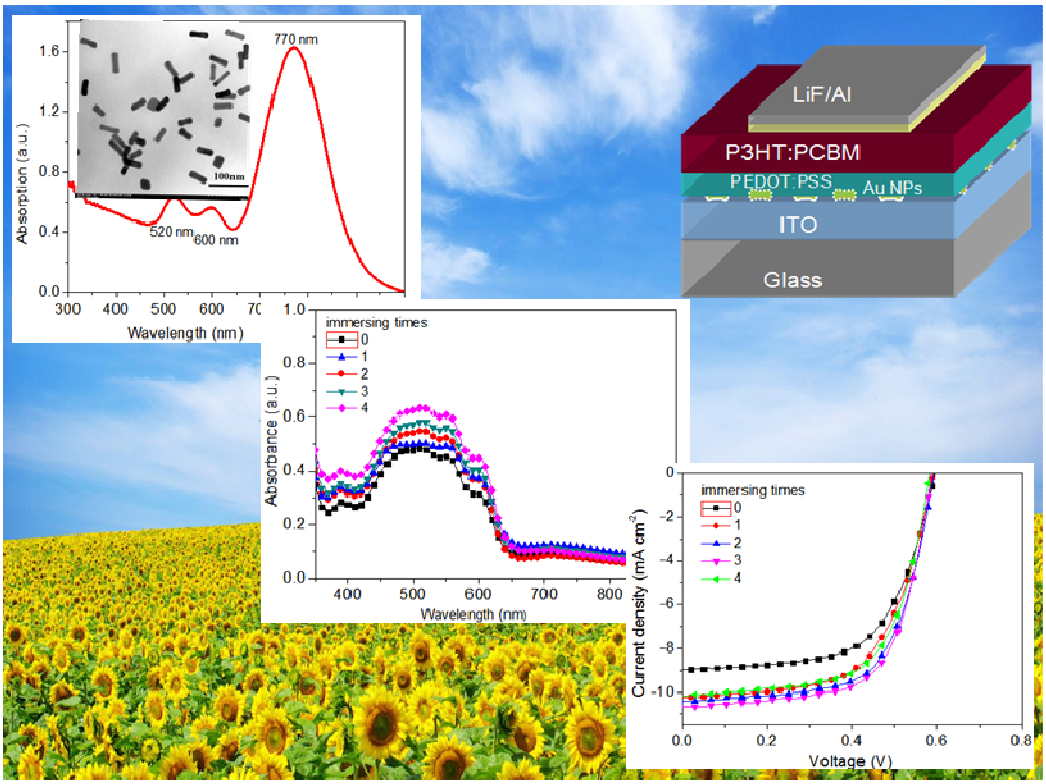

The short text for the TOC:

Mixed Au nanoparticles (NPs) with a majority of bone-like shapes and a small number of rod, cube and irregular shapes, generating wide absorption spectra of 300-1000 nm and three main absorption peaks of 520, 600, and 770 nm, are assembled onto the ITO anode to improve power conversion efficiency (PCE) in poly (3-hexylthiophene):[6,6]-phenyl-C_{61}-butyric acid methylester-based polymer solar cells. With an optimal Au NPs distribution density, significant enhancement factors of 24.2% and 18.6% for PCE and the short-circuit current are observed.

Cite this: DOI: 10.1039/c0xx00000x

www.rsc.org/xxxxxx

ARTICLE TYPE

Plasmonic-enhanced polymer photovoltaic cells based on Au nanoparticles with wide absorption spectra of 300-1000 nm

Yupei Zhang[a], Jingyu Hao[a], Xue Li[b], Shufen Chen*[a], Lianhui Wang[a], Xingao Li[a], and Wei Huang*[a,c]

Received (in XXX, XXX) Xth XXXXXXXXX 20XX, Accepted Xth XXXXXXXXX 20XX

DOI: 10.1039/b000000x

Bone-like Au nanoparticles (NPs) together with a small number of by-products of nanorods, nanocubes and other irregular shapes were synthesized with a seed-mediated growth approach. The mixed Au NPs generate very wide absorption spectra of 300-1000 nm with three main absorption peaks of 520, 600, and 770 nm respectively extending to the main absorption, cut-off and transparence region of the poly (3-hexylthiophene) (P3HT) and [6,6]-phenyl-C61-butyric acid methylester (PCBM) active layer. The mixed Au NPs were attached onto the ITO anode through a self-assembly method and then P3HT:PCBM-based polymer photovoltaic cells (OPVs) were fabricated. The short-circuit current density and power conversion efficiency exhibit significant enhancement factors of 18.6% and 24.2% accompanying with the optimization of NPs distribution density. Optical, electrical, and morphology changes with the incorporation of Au NPs in the cells were analyzed detailedly and results demonstrated that the cell performance improvement is mainly attributed to a synergistic reaction including both the localized surface plasmon resonance- and scattering-induced absorption enhancement of the active layer, Au NPs-induced hole extraction ability enhancement, and large interface roughness-induced efficient exciton dissociation and hole collection.

1. Introduction

Organic photovoltaic (OPV) cells are attracting much attention due to their potential for low-cost and high-throughput processing.[1-2] However, compared to inorganic cells, the power conversion efficiency (PCE) in OPVs must be addressed due to limitations including absorption transparence in the near-infrared (NIR) region for most of organic/polymer active layers, low carrier mobility of organic materials, large energy loss generated with the charge separation, and mismatched energy levels between the donor and the accepter. Therefore, promoting light absorption is one of key points to raise the PCE. Using new materials with low band gaps has efficiently promoted light absorption in the NIR region.[3-6] Another effective approach to enhance absorption in an active layer is utilizing surface plasmon polaritons (SPPs),[7,8] which has been widely reported in inorganic photovoltaic cells,[9,10] OPVs,[11,12] and dye-sensitized solar cells[13,14] in recent years.

SPPs are electromagnetic surface waves confined to a metal-dielectric interface by coupling to the free electron plasma in metals, which are localized around metal nanoparticles (noted with localized surface plasmon resonance, LSPR) or propagate along with planar metal surfaces. Spherical Ag or Au nanoparticles (NPs)-induced absorption enhancement has been mainly reported in OPVs in the past several years.[15-17] But the photocurrent enhancement from spherical Ag or Au nanoparticles is restricted due to a limited resonance region around 430 nm and 530 nm, respectively.[18] Some other Au NPs shapes such as triangular[17,19] and octahedron[20] have also been designed and applied in OPVs, but their LSPR peaks are still localized around 550 nm, thus restraining a further effective performance enhancement. Recently, Au NPs with asymmetrical structures have attracted much attention due to adjustable absorption spectra, simple processing technology, low manufacturing cost, etc. Rod shape Ag and Au nanostructures are becoming attractive candidates due to tunable longitudinal plasmon resonance wavelength from visible, NIR to the infrared region by simply manipulating the aspect ratios of the rods,[21,22] providing a unique opportunity for utilizing the low energy range of the solar light spectrum. In addition, Ag or Au nanorods (NRs) can be processed through wet chemical synthesis,[23] with which a well-dispersion of these NRs in a variety of aqueous/organic solutions can be simply realized. Simultaneously, their size, shape, and density can be easily controlled.[24-26] It should be pointed out that this approach of obtaining Ag or Au NRs provides a less expensive cost compared to the preparation of metal nanostructures with other methods, e.g., laser ablation,[27,28] electron beam lithography,[29] focused ion beam milling,[30] scanning tunneling microscopy assisted nanostructure formation,[31] et al. Bone-like Au NPs, owning all advantages of Au NRs, can also generate a strong local electric field intensity around the end of the bone. But their application in OPVs has not been reported up to now.

In this letter, we synthesized mixed Au NPs with a majority of bone-like shape and a small number of rod, cube and irregular shapes and then introduced them into the OPV's hole extraction layer to observe their influence on the device performances. Note that the bone-like Au NPs together with the minority of NRs, nanocubes and other irregular shapes generate a very wide

resonance absorption spectrum of 300-1000 nm with three main absorption peaks of 520, 600, and 770 nm. The absorption spectrum covers not only the main absorption region of the active layer poly(3-hexylthiophene): [6,6]-phenyl-C60-butyric acid methyl ester (P3HT:PCBM), but also the cut-off and transparence region of the active layer, therefore it will be especially beneficial to the enhancement in PCE. Another highlight in this letter is using self-assemble approach to acquire a well distribution and a good controllability for Au NPs. Moreover, self-assemble approach[32] is also a good choice for great cost saving of Au raw material. After optimizing the Au NPs' distribution density onto the ITO electrode, we realize 24.2% and 18.6% enhancement in PCE and short-circuit current intensity (J_{sc}), and this result is among the highest enhancement factor in the case of OPVs with metal NPs being doped into carrier extraction layers.

2. Materials and methods

2.1 Materials

Hydrogen tetrachloroaurate (III) trihydrate ($HAuCl_4 \cdot 3H_2O$, ≥99.9%), ascorbic acid (AA, 99%) were purchased from J&K, and sodium borohydride ($NaBH_4$, ≥99%), cetyltrimethylammonium bromide (CTAB, ≥99%)), and silver nitrate ($AgNO_3$, ≥99%) were purchased from Sigma-Aldrich. Linear polyethyleneimine (PEI, with a Mw of ~750,000, 50 wt% in H_2O) and poly (sodium-4-styrenesulfonate) (PSS, Mw of ~70,000, 30 wt% in H_2O) were purchased from Sigma-Aldrich and respectively diluted in 1 mM NaCl solution. Ultrapure deionized water (18.2 MΩ cm^{-2}) was used for all solution preparations and experiments.

2.2 Synthesis of Au NPs

Au NPs were first synthesized in aqueous solution using the colloidal seed-mediated approach according to Murphy ' s Method.[23] Detailed steps are as below: Preparation of Au seeds. 0.25 mL of an aqueous 0.01 M $HAuCl_4 \cdot 3H_2O$ solution was added to 7.5 mL of a 0.10 M CTAB solution in a glass tube. Then, 0.6 mL of 0.01 M ice-cold $NaBH_4$ solution was quickly added into the above mentioned mixed solution, followed by rapid inversion mixing for 2 minutes. The solution developed a pale brown-yellow color and was maintained in a test tube at 25 ℃. This seed solution was used 2 hours after its preparation.

Synthesis of Au NPs. 0.20 mL of a 0.01 M $HAuCl_4 \cdot 3H_2O$ aqueous solution was added into 9.5 mL of a 0.10 M CTAB solution in a glass tube. Then 0.07 mL of a 0.01 M $AgNO_3$ solution was added into the above solution with a gentle mixing. Then, 0.06 mL of a 0.10 M AA was slowly added into the mixed solution with a speed rate of one drop per 5 s. The solution became colorless upon the addition of AA. Finally, 0.02 mL of the seeded solution was added, and then reaction solution was gently mixed for 10 s and left undisturbed for at least 3 hours.

Fig. 1 (a) shows the transmission electron microscopy (TEM) image of as-synthesized Au NPs, from which one observes that besides the majority of bone-like Au NPs, a small number of NRs, nanocubes and other irregular shapes as by-products also occur. The lengths of longitudinal and transverse axes for most of the bone-like and rod shape NPs are around 45 ± 5 and 13 ± 3 nm, while the bone edge width are about 15 ± 2 nm. For the cubes, their average side length is around 30 ± 4 nm. The measured extinction spectra of the Au NPs shown in Fig. 1 (b) cover a very wide wavelength region of 300-1000 nm with three main absorption peaks of 520, 600, and 770 nm. We used finite difference time domain (FDTD) software from Lumerical Solutions Inc. to simulate the absorption cross sections around the bone, rod, and cube NPs, with results also shown in Fig. 1 (b). And simulated results demonstrate that the peaks around 770 and 520 nm mainly come from the resonances of longitudinal and transverse axes of bones and rods. From the results in Fig. 1(b), one observes that one major absorption peak in the measured absorption spectra is around 770 nm with a wide full width at half maximum (FWHM) of 153 nm, far broader than 40-50 nm of rods (the curves with magenta and dark yellow colors are rods with longitudinal and transverse axes of 40/14 and 46/12 nm, respectively) and 60-70 nm of bone-like shapes (the curves with dark, red, green, and blue colors are the bone-like shape NPs with longitudinal and transverse axes of 46/12, 45/12, 45/13, and 45/16 nm, respectively, and an edge width of 15 nm), so we conclude that the 770 nm peak is composed of some rod and bone shape NPs with a ratio range of 2.8-4.0. The 525 nm peak value corresponds to the resonance peak of the transverse axis for the rod and bone shape NPs. In our simulation result, we cannot observe the resonance from the transverse axis mainly due to the assumption that all Au NPs lie in the aqueous solution (with the longitudinal axis perpendicular to the incident light source) and this is not well matched with the real status of Au NPs (random distribution) in the water. In contrast, if we supposed that all Au NPs stand in the solution, that is, the longitudinal axis is parallel to the incident light source, the intensity from the transverse axis is far higher than that from the longitudinal axis (not attached here). For the resonance around 600 nm, it is mainly attributed to nanocube shapes with side lengths of 30 ± 4 nm.

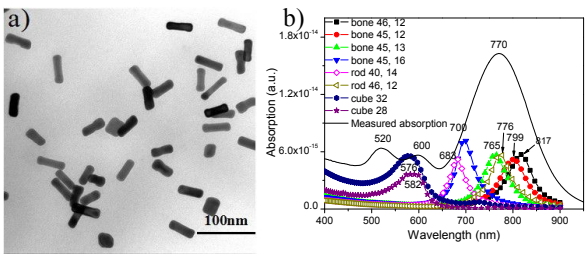

Fig. 1 a) The TEM image of as-synthesized Au NPs with a seed-mediated growth method. b) The measured and simulated absorption spectra of Au NPs.

It should be pointed out that the above absorption spectrum was measured with NPs dispersed into aqueous solution, while for the case of the Au NPs in the cells, they were assembled onto ITO and covered with a poly(3,4-ethylenedioxythiophene):poly(4-styrenesulfonate) (PEDOT:PSS) hole extraction layer, so their absorption spectra will generate a redshift due to a larger refractive index of PEDOT:PSS (~1.5) than ~1.3 of water. Thus we simulated the absorption cross sections of some representative NPs structures occurred in this paper, e.g., the bone-like Au NPs with longitudinal/transverse axes of 45/13 nm and the edge width of 15 nm, the rod ones with longitudinal/transverse axes of 46/12 and 40/14 nm, and the cube one with side length of 28 nm. The absorption cross sections for these NPs in the PEDOT:PSS film are summarized in Fig. 2 and simultaneously compared with those in aqueous solution, from which one observes that ~60 nm absorption redshift occurs in the films for all types of Au NPs. That means the resonance peak of ~600 nm in aqueous solution will move to ~660 nm in the film, while the longitudinal resonant peaks of ~770 nm in aqueous solution will shift to ~830 nm in the film, respectively corresponding to the absorption-edge (~650 nm) and the transparence zone (>700 nm) of the active layer P3HT: PCBM. According to Hsiao,[33] Li,[34] and Lu's[35] research work, the

Cite this: DOI: 10.1039/cOxxOOOOOx

www.rsc.org/xxxxxx

ARTICLE TYPE

integration of two kinds of metal NPs or metal NPs with metal nanostructures with complementary absorption spectra is beneficial to the performance enhancement in OPVs. In addition, as the analysis from Hsiao et al.,[33] the integration of NPs covering the whole absorption band-edge of the active layer is especially beneficial to the acquirement of a high enhancement factor in OPVs. Our mixed NPs cover not only the whole absorption band but also the absorption-edge and transparence zone of the active layer, indicating the effective absorption enhancement induced by LSPR will be beneficial to the performance enhancement in our solar cells.

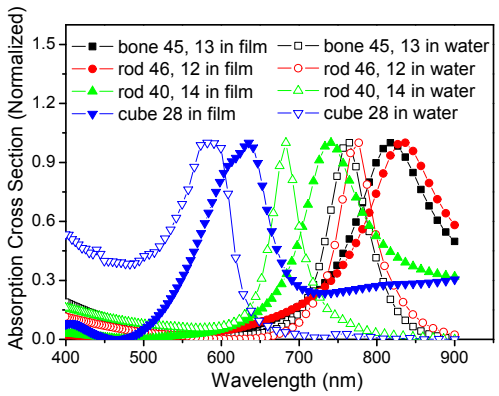

Fig. 2 Comparison of the absorption cross sections of Au NPs in the PEDOT:PSS film and in water.

2.3 Self-assemble of Au NPs onto ITO

The as-synthesized Au NPs solution was centrifuged two times at 9000 rpm (10 minutes) to remove the raw materials and reactants. To maintain a positive charge environment around the Au NPs, 1 mL of a 0.10 M CTAB aqueous solution was added into the Au NPs solution.

ITO glass substrates were sonicated in sequence in acetone, ethanol, and deionized water for 10 min, respectively. After blown with nitrogen gas, the dried substrates were first immersed into the 10 mM PEI solution (containing 0.01 mM NaCl) for 2 h to introduce positive charges onto the ITO surface, then immersed into 10 mM PSS aqueous solution (containing 0.01 mM NaCl) for 2 h to introduce negative charges onto the substrate surface. After exhaustive rinsing with water and drying with nitrogen gas, the substrates were immersed into the Au NPs solution for 12 h, forming the self-assembled Au NPs structures.[32] To increase the self-assembled Au NPs density, the ITO glass substrates were immersed again into the PSS aqueous solution for 20 min and then into the Au NPs solution for 40 min, which corresponds to immersing times of 2.[36] In this paper, we scanned the Au NPs distributions on ITO with immersing times of 1, 2, 3, and 4 with scanning electron microscopy (SEM) and explored the influence of different immersing times on the cell performances. As exhibited in Fig. 2, the Au NPs density obviously increases with the immersing times. We also observe that almost all Au NPs with bone or rod shapes lie onto the ITO substrates and no apparent aggregation of the Au NPs is found using this simple method.

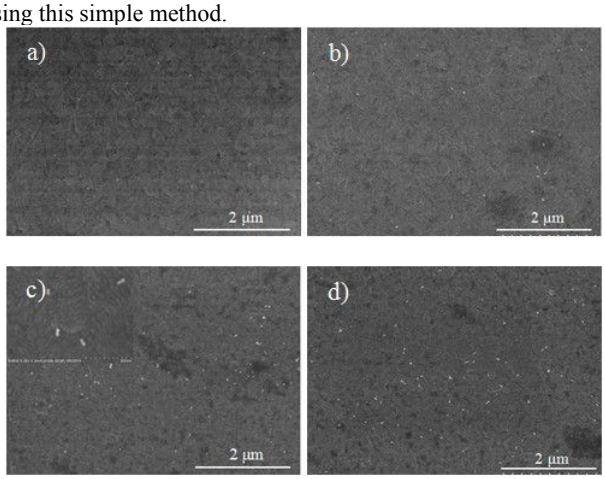

Fig. 3 SEM images for the self-assembled Au NPs onto the ITO-coated glass substrate. a), b), c), and d) correspond to the immersing times of 1, 2, 3, and 4.

2.4 Device fabrication and characterization

The ITO substrates covered with the self-assembled Au NPs were treated first with an ultraviolet light for 3 min. Then another PEDOT:PSS hole extraction layer was spin-coated onto ITO with an annealing process of 100 ℃ for 15 min. The polymer blend solution was prepared by mixing P3HT and PCBM with 1:1 weight ratio in dichlorobenzene with a total concentration of 30 mg ml^{-1}. The mixed solution was spin-coated onto the PEDOT:PSS layer at 800 rpm for 36 s to form the active layer, followed by a solvent annealing process of 1.5 h. The final thickness of the active layer is about 70 nm. Finally, a 1 nm LiF ultrathin film as the electron extraction layer and a 100 nm Al layer as the cathode were sequentially evaporated onto the active layer. Fig. 4 shows the architectures of our plasmonic-enhanced OPV device and the control device.

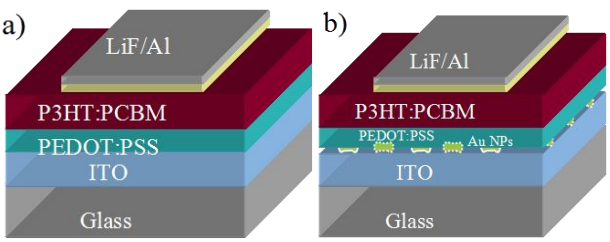

Fig. 4 Device structures of without a) and with b) Au NPs.

3. Results and discussion

Changing the times immersed in Au NPs' solution to alter the distribution density of Au NPs is firstly discussed. As shown in Fig. 3, the NPs' distribution density significantly increases with the immersing times. Current density-voltage (*J-V*) characteristics for four groups of OPV devices with different Au

Cite this: DOI: 10.1039/cOxx00000x

www.rsc.org/xxxxxx

ARTICLE TYPE

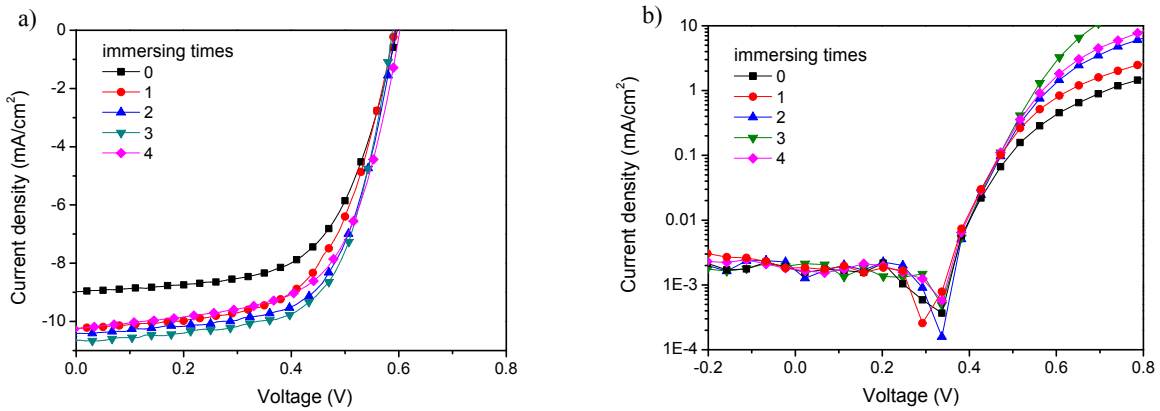

Fig. 5 The *J-V* curves for all devices measured under illumination a) and in dark b) conditions.

Table 1 Performances of the devices

Immersing times	*V*oc (V)	*J*sc (mA cm^{-2})	FF (%)	PCE (%)	*R*s (Ω cm^2)
W/O Au NPs	0.60±0.01	8.97±0.08	60.8±0.30	3.27±0.04	10.89±1.76
1	0.60±0.01	10.23±0.12	59.9±0.43	3.68±0.24	10.22±1.08
2	0.60±0.02	10.41±0.15	63.7±0.06	3.97±0.14	9.56±1.59
3	0.59±0.02	10.64±0.05	64.7±0.03	4.06±0.04	8.44±1.08
4	0.59±0.01	10.19±018	63.2±0.02	3.81±0.12	9.38±2.03

NPs density distributions are presented in Fig. 5 and the photovoltaic parameters are summarized in Table 1. These data are obtained from more than 20 groups of devices for each structure. Analysis demonstrates that assembling Au NPs helps to enhance both J_{sc} and PCE. The device immersed with three times realizes a maximum J_{sc} and PCE of 10.64 mA cm^{-2} and 4.06%, with enhancement factors of 18.6% and 24.2% compared to those in the control device. With a low density of Au NPs, FF shows a slight decrease and then begins to increase along with the increase in the Au NPs density. A maximum FF value occurs at three times with a distribution density of 2.5×10^7 NPs cm^{-2}. The introduction of a small number of NPs onto the ITO electrode surface almost unaffects the open-circuit voltage (V_{oc}), and with a further increase in distribution density of Au NPs, V_{oc} shows a very slight decline. A proper NPs density also reduces the series resistance (R_S) in the cells mainly due to two reasons below. On one hand, a higher work function of Au (5.4 eV) than the highest occupied molecular orbital (~5.2 eV) of PEDOT:PSS provides with a fine hole extraction ability at the ITO/PEDOT:PSS interface. On the other hand, the Au NPs simultaneously generate a shallow impurity energy level in the PEDOT:PSS film.[37, 38]The single hole devices with and without Au NPs were fabricated to observe the influence of Au NPs doping on the hole transport ability of the PEDOT:PSS film. Result indicates that it forms an ohmic contact at both the interfaces of ITO/PEDOT:PSS and ITO/Au NPs-doped PEDOT:PSS. The incorporation of Au NPs efficiently decreases the resistance of the PEDOT:PSS film, resulting in the increase in current density under a same driving bias. And this point is also consistent with dark *J-V* characteristics (Fig. 5b), in which *R*s and *J* are respectively decreased and enhanced with a high Au NPs distribution density.

Fig. 6 shows the incident photon-to-electron conversion efficiency (IPCE) data for the OPV devices with different NPs immersing times. The corresponding IPCE curves with different immersing times exhibit an obvious improvement over a wide wavelength range of 380-650 nm compared to that in the standard device, consistent with the above measured *J-V* characteristics and similar with other's report result.[16, 39] The improvement on IPCE can be attributed to many factors including electrical and optical improvements. As discussed above, the decrease in the resistance of the PEDOT:PSS film is helpful to transport the dissociated holes. Meanwhile the higher work function of Au than ITO is beneficial to extract holes into the anodes. In addition, the absorption spectra of the multilayer films of Au NPs/PEDOT:PSS/P3HT:PCBM and the control film of PEDOT:PSS/P3HT:PCBM were also measured to observe

Cite this: DOI: 10.1039/cOxxOOOOOx

www.rsc.org/xxxxxx

ARTICLE TYPE

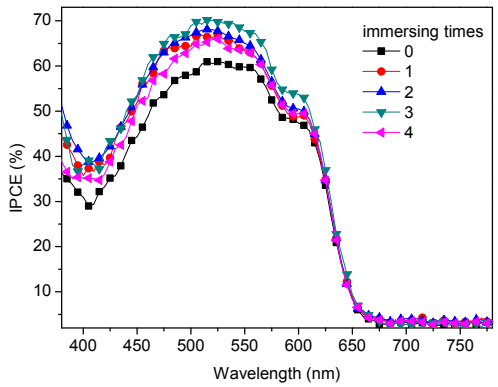

Fig. 6 IPCE curves for the OPV devices with different NPs immersing times.

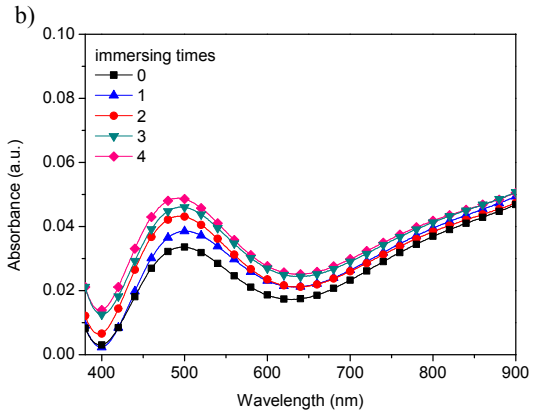

Fig. 7 Absorbance of the a) PEDOT:PSS/P3HT:PCBM film and b) PEDOT:PSS film with (immersing times from 1 to 4) or without Au NPs incorporation. The inset shows the absorption difference between A_3 (Au NPs with immersing three times PEDOT:PSS/P3HT:PCBM) and A_0 (PEDOT:PSS/P3HT:PCBM).

the LSPR-induced absorption enhancement.

As shown in Fig. 7a, the light absorption around 350-650 nm is continuously enhanced along with the increase in Au NPs density. This enhancement can be attributed to the absorption increase of the active layer and the PEDOT:PSS extraction layer induced by the LSPR of Au NPs. To observe the absorption change in the PEDOT:PSS extraction layer, the light absorption of only Au NPs/PEDOT:PSS (Fig. 7b) is measured and the results demonstrate that the absorption from PEDOT:PSS shows some increase accompanying with the introduction of Au NPs, indicating some light enhancement occurs in PEDOT:PSS that is not contributed to the photocarrier generation. But fortunately, these increase is relatively weak comparable to that in the active layer, indicating the main absorption enhancement comes from the active layer induced by LSPR. Besides that, refers to the absorption difference between A_3 (Au NPs with immersing three times/P3HT:PCBM) and A_0 (P3HT:PCBM) shown in the inset of Fig. 7b, another minor absorption shoulder around 740 nm is observed, which is mainly due to a direct absorption of the bone or rod Au NPs with large aspect ratios to the incident light. However, this part of absorption gives no help to the increase in IPCE around 740 nm due to the transparence of the absorption of the active layer. But fortunately, the NPs with larger sizes bring a strong scattering to the incident light and generate a lengthened light transport path, resulting in a further increase in light absorption in OPV cells. The incorporation of the Au NPs increasing the light harvesting in the devices is further testified with the significant intensity enhancement in the photoluminescence (PL) spectra (Fig. 8). With the increase in immersing times, the PL spectra for Au NPs/PEDOT:PSS/P3HT:PCBM exhibits a significant raise in intensity. We attribute the enhanced PL intensity to the fact that excitation of the LSPR increases the degree of light absorption and, thereby, enhances the light excitation rate.[40] In addition, according to the previous report,[16] to the absorption enhancement, the exciton quenching with non-radiative energy transfer at metal/active layer interfaces also changes the PL

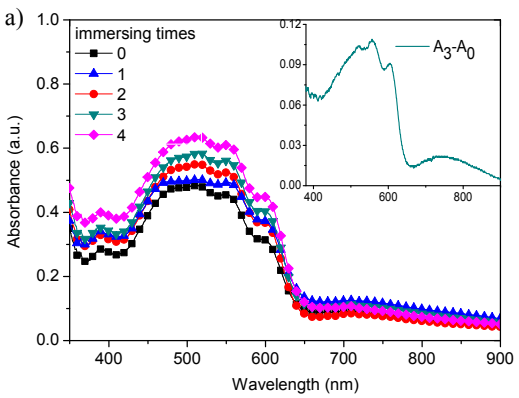

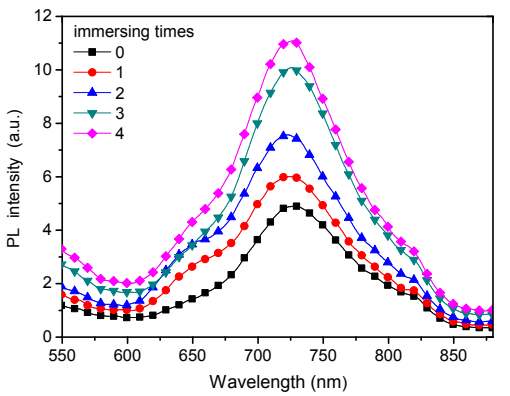

Fig. 8 PL spectra of Au NPs/PEDOT:PSS/P3HT:PCBM with different immersing times. Here, a standard PL spectrum without Au NPs is for comparison.

intensity. Our PL results indicate no obvious PL quenching phenomenon occurs in the active layer due to efficiently wrapping NPs with CTAB and PEDOT:PSS. Another possible factor affecting the PL intensity is the morphology change of films, so we measured the XRD profiles of P3HT:PCBM films and observed the influence of the introduction of Au NPs on the film morphology. From Fig. 9, we clearly observed that the intensity of the (100) peak (corresponds to the diffraction peak of 5.4°) increases together with the decline in the FWHM of (100) diffraction spectrum with the utilization of Au NPs, indicating that the number of P3HT crystallites increase and the film has closer P3HT chains. Here, closer P3HT chains distance suggests a lower resistance to the hopping of carriers between P3HT backbones, which results in a higher *J*sc and a smaller *R*s than the reference devices.[41]

In addition to the absorbance enhancement in the NPs-modified OPVs and the alteration of the hole extraction and transport ability induced by Au NPs, other possible factors, e.g., the influence of incorporating Au NPs on the morphology changes of the PEDOT:PSS film, have been further investigated to observe their influences on solar cells. It has been suggested that a rough P3HT:PCBM surface creates defect sites that assist exciton dissociation.[42] Moreover, increasing anode surface roughness will increase the interface area between the anode and the active layer, providing shorter routes for holes to travel to the anode and enhancing hole collection at the anode.[43] The increased

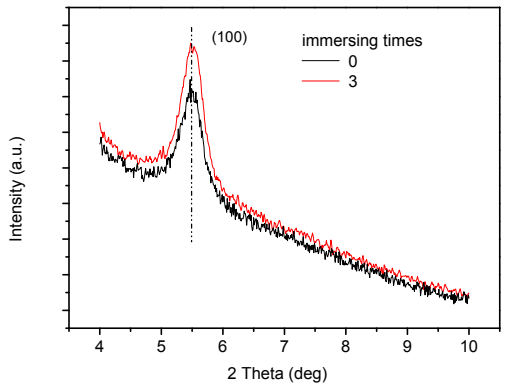

Fig. 9 XRD profiles of P3HT:PCBM films with (immersing times of 3) and without Au NPs.

interfacial area between PEDOT:PSS and P3HT:PCBM allows the collection of a larger number of holes in the P3HT:PCBM layer, thus increasing J_{sc}. Thus, the morphology changes of the PEDOT:PSS layer with different Au NPs density are measured by applying Atomic Force Microscopy (AFM) on the PEDOT:PSS film, as shown in Fig. 10. With introducing the Au NPs, we observe an obvious surface morphology change of the NPs/PEDOT:PSS film with an increase in surface roughness (R_a) from 0.55 nm for the pure PEDOT:PSS film to 1.025 nm for the Au NPs-assembled PEDOT:PSS film with immersing times of 3. This result indicates that the introduction of NPs is beneficial to exciton dissociation and the collection of a larger number of holes to some extent, resulting in the increase in J_{sc}. The obvious phase separation for the P3HT:PCBM films after assembling the Au NPs is also helpful to the carrier transport, thus the J_{sc} increase.

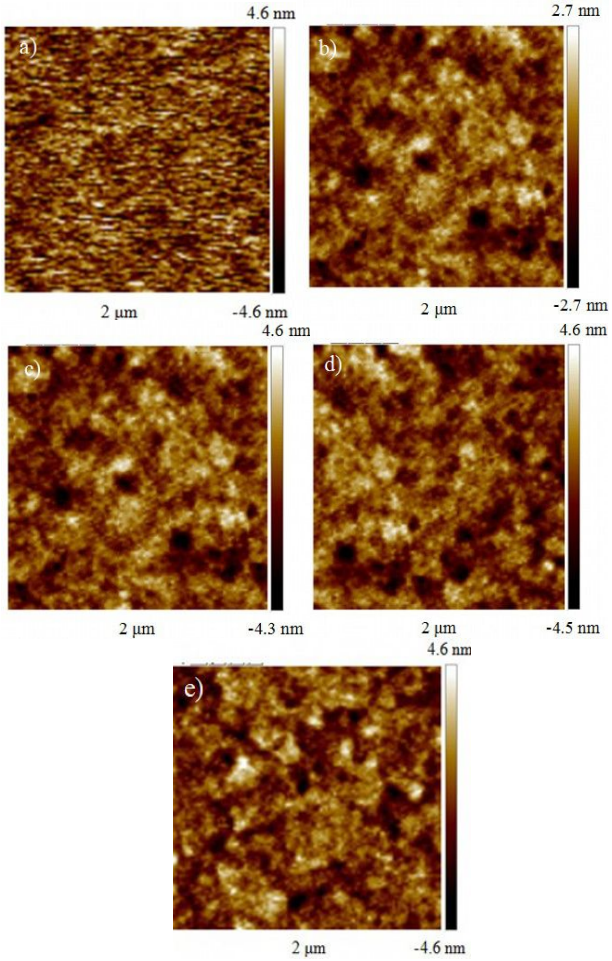

Fig. 10 AFM images of the pure PEDOT:PSS film and the Au NPs-assembled PEDOT:PSS film with different immersing times. a) 0, R_a=0.550, b) 1 time, R_a=0.590, c) 2 times, R_a=0.996, d) 3 times, R_a=1.025, and e) 4 times, R_a=0.973.

4. Conclusions

In conclusion, we synthesized mixed Au NPs with a majority of bone-like Au NPs together with a small number of rod, cube and irregular shapes with a seed-mediated growth approach. It is noted that the mixed Au NPs generate a very wide absorption spectrum of 300-1000 nm with three main absorption peaks of 520, 600, and 770 nm. For the first time, we assembled the mixed Au NPs with a wide absorption spectrum on the ITO anode and fabricated polymer photovoltaic cells with P3HT:PCBM as the active layer, in which J_{sc} and PCE show significant enhancement factors of 18.6% and 24.2% with the optimization of Au NPs distribution density. We explored optical, electrical, and morphology changes with the incorporation of Au NPs in the cells and research results demonstrated that the cell performance improvement can be attributed to a synergistic reaction including 1) both the localized surface plasmon resonance- and scattering-induced absorption enhancement of the active layer, 2) Au NPs-induced hole extraction ability enhancement, and 3) large interface roughness-induced efficient exciton dissociation and hole collection.

Acknowledgements

Cite this: DOI: 10.1039/cOxxOOOOOx

www.rsc.org/xxxxxx

ARTICLE TYPE

The authors acknowledge financial support from the Ministry of Science and Technology (973 project, Grant No. 2012CB933301), NSFC (Grant Nos. 61274065, 60907047, 51173081, 61136003, 51372119, 51172110, and BZ2010043), the Ministry of Education of China (No. IRT1148), the Research Projects of the Social Science and Humanity on Young Fund of the Ministry of Education (Grant No. 13YJCZH091), the "Qing Lan" Program of Jiangsu Province, the Priority Academic Program Development of Jiangsu Higher Education Institutions, and Synergetic Innovation Center for Organic Electronics and Information Displays.

Notes and references

[a] *Key Laboratory for Organic Electronics and Information Displays (KLOEID) and Institute of Advanced Materials (IAM), Nanjing University of Posts and Telecommunications (NUPT), Nanjing, 210023, P. R. China. E-mail: iamsfchen@njupt.edu.cn.*
[b] *Mechanical Engineering Institute, Nanjing Institute of Technology, Nanjing 211167, China*
[c] *Jiangsu-Singapore Joint Research Center for Organic/Bio-Electronics & Information Displays and Institute of Advanced Materials, Nanjing Tech University, Nanjing 211816, China.*
E-mail: iamdirector@fudan.edu.cn.

1 Z. C. He, C. M. Zhong, S. J. Su, M. Xu, H. B. Wu and Y. Cao, *Nat. Photon.*, 2012, **6**, 591-595.
2 M. A. Green, K. Emery, Y. Hishikawa, W. Warta and E. D. Dunlop, *Prog. Photovolt: Res. Appl.,* 2012, **20**, 12-20.
3 M. C. Daniel and D. Astruc, *Chem. Rev.*, 2004, **104**, 293-346.
4 X. S. Kou, S. Z. Zhang, C. K. Tsung, Z. Yang, M. H. Yeung, G. D. Stucky, L. D. Sun, J. F. Wang and C. H. Yan, *Chem. Eur. J.*, 2007, **13**, 2929-2936.
5 W. Ni, X. Kou, Z. Yang and J. F. Wang, *ACS Nano*, 2008, **2**, 677-686.
6 N. R. Jana, L. Gearheart and C. J. Murphy, *J. Phys. Chem. B.,* 2001, **105**, 4065-4067.
7 Q. Q. Gan, F. J. Bartoli and Z. H. Kafafi, *Adv. Mater.*, 2013, **25**, 2385-2396.
8 E. Stratakis and E. Kymakis, *Mater. Today*, 2013, **16**,133-146.
9 D. Derkacs, W. V. Chen, P. M. Matheu, S. H. Lim, P. K. L. Yu and E. T. Yu, *Appl. Phys. Lett.*, 2008, **97**, 091107.
10 R. A. Pala, J. White, E. Barnard, J. Liu and M. L. Brongersma, *Adv. Mater.*, 2009, **21**, 3504-3509.
11 F. X. Xie, W. C. H. Choy, C. C. D. Wang, W. E. I. Sha and D. D. S. Fung, *Appl. Phys. Lett.*, 2011, **99**, 153304.
12 T. Okamoto and I. Yamaguchi, *J. Phys. Chem.* B, 2003, **107**, 10321-10324.
13 C. Wen, K. Ishikawa, M. Kishima and K. Yamada, *Sol. Energy Mater. Sol. Cells*, 2000, **61**, 339-351.
14 C. Hägglund, M. Zäch and B. Kasemo, *Appl. Phys. Lett.*, 2008, **92**, 013113.
15 J. H. Lee, J. H. Park, J. S. Kim, D. Y. Lee and K. Cho, *Org. Electron.*, 2009, **10**, 416-420.
16 D. D. S. Fung, L. F. Qiao, W. C. H. Choy, C. D. Wang, W. E. I. Sha, F. X. Xie and S. L. He, *J. Mater. Chem.*, 2011, **21**, 16349-16356.
17 X. H. Li, W. C. H. Choy, H. F. Lu, W. E. I. Sha and A. H. P. Ho *Adv. Funct. Mater.*, 2013, **23**, 2728-2735.
18 M.-C. Daniel and D. Astruc, *Chem. Rev.*, 2004, **104**, 293.
19 C. Xue, Z. Li and C. A. Mirkin, *Small*, 2005, **1**, 513-516.
20 W.-L. Liu, F.-C. Lin, Y.-C. Yang, C.-H. Huang, S. Gwo, M. H. Huang and J.-S. Huang, *Nanoscale*, 2013, **5**, 7953–7962.
21 X. S. Kou, S. Z. Zhang, C. K. Tsung, Z. Yang, M. H. Yeung, G. D. Stucky, L. D. Sun, J. F. Wang and C. H. Yan, *Chem. Eur. J.*, 2007, **13**, 2929-2936.
22 J. Pérez-Juste, I. Pastoriza-Santos, L. M. Liz-Marzán and P. Mulvaney, *Coord. Chem. Rev.*, 2005, **249**, 1870.
23 T. K. Sau and C. J. Murphy, *Langmuir*, 2004, **20**, 6414-6420.
24 B. Nikoobakht and M. A. El-Sayed, *J. Phys. Chem.* A, 2003, **107**, 3372-3378.
25 W. A. Murray and W.L. Barnes, *Adv. Mater.*, 2007, **19**, 3771-3782.
26 M. Pelton, J. Aizpurua and G. Bryant, *Laser & Photon. Rev.*, 2008, **2**, 136-159.
27 C. D. Chen, Y. T. Yeh and C. R. C. Wang, *J. Phys. Chem. Solids.*, 2001, **62**, 1587-1597.
28 J. Bosbach, D. Martin, F. Stietz, T. Wenzel and F. Trager, *Appl. Phys. Lett.*, 1999, **74**, 2605.
29 N. Felidj, J. Aubard, G. Levi, J. R. Krenn, M. Salerno, G. Schider, B. Lamprecht, A. Leitner and F. R. Aussenegg, *Phys. Rev. B*, 2002, **65**, 075419.
30 Y. C. Chang, F. Y. Chou, P. H. Yeh, H. W. Chen, S. H. Chang, Y. C. Lan, T. F. Guo, T. C. Tsai and C. T. Lee, *J. Vac. Sci.*, 2007, **25**, 1899-1902.
31 D. M. Kolb, R. Ullmann and T. Will, *Science*, 1997, **275**, 1097-1099.
32 A. Gole and C. J. Murphy, *Chem. Mater.*, 2005, **17**, 1325-1330.
33 Y.-S. Hsiao, S. Charan, F.-Y. Wu, F.-C. Chien, C.-W. Chu, P. Chen and F.-C. Chen, *J. Phys. Chem. C*, 2012, **116**, 20731-20737.
34 X. Li, W. C. H. Choy, L. Huo, F. Xie, W. E. I. Sha, B. Ding, X. Guo, Y. Li, J. Hou, J. You and Y. Yang, *Adv. Mater.*, 2012, **24**, 3046-3052.
35 L. Y. Lu, Z. Q. Luo, T. Xu and L. P. Yu, *Nano Lett.*, 2013, **13**, 59-64.
36 X. G. Hu, T. Wang and S. J. Dong, *J. Colloid Interface Sci.*, 2007, **316**, 947-953.
37 K. Kim and D. L. Carroll, *Appl. Phys. Lett.*, 2005, **87**, 203113.
38 C. C. D. Wang, W. C. H. Choy, C. Duan, D. D. S. Fung, W. E. I. Sha, F.-X. Xie, F. Huang and Y. Cao, *J. Mater. Chem.*, 2012, **22**, 1206-1211.
39 S.-S. Kim, S.-I. Na, J. Jo, D.-Y. Kim and Y.-C. Nah, *Appl. Phys. Lett.*, 2008, **93**, 073307.
40 J.-Lih Wu, F. -C. Chen,Y.-S. Hsiao, F. -C. Chien, P. Chen,C. -H. Kuo, M. H. Huang and C. -S. Hsu, *ACS Nano*, 2011, **5**, 959-967.
41 D. Kekuda, H.-Shing Lin,M. C. Wu, J.-S. Huang, K.-C. Ho, C-W.Chu, *Sol. Energy Mater. Sol. Cells*, 2011, **49**, 419-422.
42 G. Li, V. Shrotriya, Y. Yao and Y. Yang, *J. Appl. Phys.*, 2005, **98**, 043704.
43 M.-H. Hsu, P. Yu, J.-H. Huang, C.-H. Chang, C.-W. Wu, Y.-C. Cheng and C.-W. Chu, *Appl. Phys. Lett.*, 2011, **98**, 073308.